Clim. Past Discuss., 9, 3519–3561, 2013
www.clim-past-discuss.net/9/3519/2013/
doi:10.5194/cpd-9-3519-2013

Climate of the Past Discussions

Limited response of peatland CH_4 emissions to abrupt Atlantic Ocean circulation changes in glacial climates

P. O. Hopcroft[1], P. J. Valdes[1], R. Wania[2], and D. J. Beerling[3]

[1]Bristol Research Initiative for the Dynamic Global Environment (BRIDGE), School of Geographical Sciences, University of Bristol, Bristol BS8 1SS, UK
[2]Lanser Strasse 30, 6080 Igls, Austria
[3]Department of Animal and Plant Sciences, University of Sheffield, Sheffield S10 2TN, UK

Received: 23 May 2013 – Accepted: 13 June 2013 – Published: 26 June 2013

Correspondence to: P. O. Hopcroft (peter.hopcroft@bris.ac.uk)

Published by Copernicus Publications on behalf of the European Geosciences Union.

Abstract

Ice-core records show that abrupt Dansgaard-Oeschger climatic warming events of the last glacial period were accompanied by large increases in the atmospheric CH_4 concentration (up to 200 ppbv). These abrupt changes are generally regarded as arising from the effects of changes in the Atlantic Ocean meridional overturning circulation and the resultant climatic impact on natural CH_4 sources, in particular wetlands. We use two different ecosystem models of wetland CH_4 emissions to simulate northern CH_4 sources forced with coupled general circulation model simulations of five different time periods during the last glacial to investigate the potential influence of abrupt ocean circulation changes on atmospheric CH_4 levels during D-O events. The simulated warming over Greenland of 7–9 °C in the different time-periods is at the lower end of the range of 11–15 °C derived from ice-cores, but is associated with strong impacts on the hydrological cycle, especially over the North Atlantic and Europe during winter. We find that although the sensitivity of CH_4 emissions to the imposed climate varies significantly between the two ecosystem emissions models, the model simulations do not reproduce sufficient emission changes to satisfy ice-core observations of CH_4 increases during abrupt events. This suggests that alternative scenarios of climatic change could be required to explain the abrupt glacial CH_4 variations.

1 Introduction

Dansgaard-Oeschger (D-O) cycles are chiefly characterised by a series of 25 incredibly abrupt warming episodes which occurred during the last glacial period. These events have been reconstructed from Greenland ice-core data (e.g. NGRIP Project Members, 2004; Wolff et al., 2010) and from an increasing number of palaeoclimate proxies from across the globe (e.g. Peterson et al., 2000; Hendy and Kennett, 2000; Wang et al., 2001; Kanner et al., 2012). D-O events typically constitute abrupt warmings of 8 to 16 °C in Greenland which take place over 10–40 yr (e.g. Huber et al., 2006). These

CPD
9, 3519–3561, 2013

temperature transitions were also accompanied by abrupt changes in atmospheric CH_4, N_2O, dust and δD of ice (e.g. Huber et al., 2006; Wolff et al., 2010), suggesting large-scale abrupt climatic changes which present a challenge to our understanding of natural climatic variability (Seager and Battisti, 2007).

At present D-O climate events are poorly understood and there remain a number of different hypotheses of their causation (e.g. Clement and Peterson, 2008; Liu et al., 2009; Li et al., 2010; Petersen et al., 2013). The predominant theory revolves around non-linear changes in the deep-water formation in the North Atlantic Ocean associated with the Atlantic meridional overturning circulation (AMOC) and its Northwards heat transport. Abrupt climate transitions in a glacial state have been demonstrated in intermediate complexity climate models (e.g. Ganopolski and Rahmstorf, 2001), but the behaviour in fully coupled general circulation models appears fundamentally different (Liu et al., 2009), relating to changes in the strength of the AMOC rather than the latitudinal position. This is potentially as a result of the inclusion of feedbacks from a dynamic atmospheric model (Yin et al., 2006).

Atmospheric CH_4 is one of the few quantities recorded in Greenland ice (Flückiger et al., 2004; Spahni et al., 2005) which suggests widespread climatic anomalies during D-O events, and it potentially provides quantitative constraints on the nature of D-O events. Ice-core data show that CH_4 shifts during D-O warming events are large, ranging up to two thirds of the glacial-interglacial (G-IG) range, i.e. rapid increases of up to 200 ppbv (Huber et al., 2006; Flückiger et al., 2004; Wolff et al., 2010). Ice-core data on the interpolar gradient of CH_4 as well as its isotopic signature allow for top-down estimates of the changes in sources during past climate and in general suggest that wetland emissions played a significant role in past atmospheric CH_4 variations. Recent improvements in the determination of the interpolar gradient of CH_4 from ice-core measurements suggest that low latitude sources made the dominant contribution to abrupt changes in atmospheric CH_4 during the last glacial period (Baumgartner et al., 2012) in agreement with Brook et al. (2000). This is in contrast to the work of Dällenbach

CPD
9, 3519–3561, 2013

et al. (2000) who concluded that northern sources played a dominant role during these abrupt events.

Hopcroft et al. (2011) used the Sheffield Dynamic Global Vegetation Model (SDGVM) (Woodward et al., 1995; Beerling and Woodward, 2001) to simulate the global wetland CH_4 emission responses in a series of different climate simulations with large AMOC perturbations. Globally the simulated CH_4 changes translated into atmospheric increases ranging from 50 to 110 ppbv, and were considered too small to be reconciled with ice-core observations, especially the changes in emissions from the Northern hemisphere extra-tropics. By contrast the model has been used to successfully predict the longer orbital-scale changes in atmospheric CH_4 of the last 120 kyr (Singarayer et al., 2011). The weak response to abrupt changes was thought to result either from deficiencies in the climate scenario, or the sensitivity of the CH_4 emission model employed within SDGVM (modified from Cao et al., 1996). For example, SDGVM does not simulate the difference between air and soil temperatures. Hence it does not directly include the influence of freezing on soil moisture availability and does not include vertical discretisation of thermodynamics in the soil which could be crucial for correctly simulating abrupt changes in CH_4 emissions. Additionally, the climate simulations of Hopcroft et al. (2011) were idealised, pertaining either to the LGM (Last Glacial Maximum: 21 kyr BP), or to some idealised boundary conditions (e.g. LGM with altered orbital insolation). This complicated the direct comparison with D-O events which show great variability, especially in terms of the amplitude of abrupt CH_4 rises, which are thought to arise through the influence of longer-term changes in atmospheric CO_2 and orbital insolation values (e.g. Flückiger et al., 2004).

Here we focus on the potential responses of the Northern Boreal wetlands at specific time-periods relevant for understanding the D-O CH_4 anomalies. We used the FAMOUS (Smith et al., 2008), a coupled atmosphere-ocean general circulation model (GCM) to simulate the global climate of 5 time periods during the last glacial period driven by estimates of the major climatic forcings: orography, land ice and sea level, trace gases, insolation and transient changes in freshwater input. The simulated cli-

CPD
9, 3519–3561, 2013

mates are then used to drive the dynamic vegetation model LPJ-WHyMe (Wania et al., 2009a,b, 2010) and for comparison SDGVM to simulate the response of the Northern peatlands and permafrost to abrupt climate changes in the North Atlantic region. LPJ-WHyMe is a development of LPJ (Gerten et al., 2004) and includes representations of permafrost thermodynamics and hydrology and peatland carbon cycling and methane emissions. The comparison with SDGVM allows an assessment of changes to sensitivities that are caused by the presence of these additional processes as compared with a more generalised wetland CH_4 scheme. This modelling setup is used to test assumptions about the climate- CH_4 coupling of D-O warming events and to investigate the potential for constraints on mechanisms of climate change during these abrupt transitions.

2 Methods

2.1 Coupled GCM simulations

We performed a series of coupled atmosphere-ocean climate model simulations using the FAMOUS coupled general circulation model (Smith et al., 2008), a low-resolution version of HadCM3 (Gordon et al., 2000). The model is configured following the methods of Singarayer and Valdes (2010) for the time periods considered, which are: the LGM, 14, 38, 44 and 60 kyr, where the latter 4 are close to times of significant D-O events as shown in Table 1. In all simulations the ice sheets, land sea mask and sea-level are altered according to ICE-5G (Peltier, 2004), the CO_2, CH_4 and N_2O mixing ratios are prescribed based on Vostok and EPICA ice-core data (Petit et al., 1999; Spahni et al., 2005), and insolation is modified according to the orbital parameters of Berger and Loutre (1991). The vegetation distribution which is prescribed in FAMOUS, is based on the pre-industrial, but accounting for changes in land area and ice-sheet distribution. Each simulation is initialised from pre-industrial initial conditions and integrated without freshwater forcing for at least 500 yr.

CPD
9, 3519–3561, 2013

The subsequent 500 yr simulation includes a freshwater forcing scenario which is designed to produce large changes in the Atlantic meridional overturning circulation (AMOC) which drives an abrupt and large magnitude of warming over Greenland. This is consistent with previous modelling studies (e.g. Ganopolski and Rahmstorf, 2001; Liu et al., 2009; Merkel et al., 2010), though the exact mechanism of abrupt change in freshwater varies between models and is not addressed here. The freshwater input follows that used by Hopcroft et al. (2011), and is prescribed at a maximum rate of ±0.5 Sv ($1\,\mathrm{Sv} = 10^6\,\mathrm{m}^3\,\mathrm{s}^{-1}$) over the North Atlantic between 50°–70° N. This forcing leads to a shutdown to essentially no overturning circulation, followed by a reasonably rapid (100 yr) change to a circulation of approximately twice the control value in each time period. We also begin to explore the sensitivity to the freshwater forcing by including an additional LGM simulation with twice the magnitude (amplitude of 1.0 Sv) of freshwater forcing.

2.2 Peatland methane emission model

The peatland CH_4 emissions are calculated using the dynamic global vegetation model LPJ-WHyMe (Lund-Potsdam-Jena Wetland Hydrology and Methane, Wania et al., 2010) which includes representations of peatland hydrology and the thermodynamics of permafrost to 10 m (Wania et al., 2009a,b). LPJ-WHyMe includes 2 plant functional types (PFTs) corresponding to C3 graminoids and *Sphagnum* mosses which are specific to wetlands. The carbon cycle simulated within peatland gridcells is hence wetland-specific, in contrast with many previous wetland models use upland vegetation distributions as a proxy for the carbon balance in wetland grid-cells. CH_4 emissions are dependent on the methanogen available carbon pool which is calculated from exudates, above- and belowground and fast and slow carbon pools, which is then weighted by root density. The temperature dependence of microbial activity is based on an activation energy approach which gives more realistic behaviour at low temperatures compared with a formulation which employs a single Q_{10} value. CH_4 emission by plant mediated transport, ebullition (bubbling) and diffusion are modelled separately.

CPD
9, 3519–3561, 2013

LPJ-WHyMe requires monthly surface air temperatures, precipitation, cloudiness and wetdays as well as the atmospheric CO_2 concentration. In this work the prescribed CO_2 level generally takes the same value as in the respective FAMOUS GCM simulation, and output from the transient FAMOUS experiments is used for the remaining variables, with the exception of wetdays, which is not directly simulated. We calculate this field as a 12 month climatology for each model gridcell using an exponential regression of the CRU observed precipitation and wetdays (1961–1990) (New et al., 1999) applied to the precipitation climatology calculated from the initial 30 yr of each model simulation.

LPJ-WHyMe requires specification of the area considered peatland soils. The model then interactively simulates the vegetation distribution, carbon balance, hydrology and CH_4 emissions in each gridcell of peat as a function of input climate. For the pre-industrial, this peat distribution is derived from the IGBP soil map of carbon rich northern soils (Wania et al., 2009a). Pre-Holocene peatland distributions can be inferred from assemblages of peat-core radiocarbon basal dates back to around 16 kyr BP. For example, MacDonald et al. (2006) and Yu et al. (2010) derive time-slice maps of global peatland formation in northern areas and globally. These assemblages can then be extrapolated to give an estimate of the total peatland area through time, assuming linear time dependence of areal expansion around core sites (see Korhola et al., 2009 and Reyes and Cooke, 2011 for some discussion of limitations to this type of approach).

As a first order approach we took the current peatland areas and mapped these to palaeo-time periods taking account of land ice (Peltier, 2004) and areas of new land. This gives relatively good agreement with reconstructions (Yu et al., 2010), as this results in almost complete removal of North American and European peat areas at the LGM, although it has less impact on the Siberia peatland distribution. The total peat soil area is reduced by a factor of 32 %, but the reduction is more extreme in North America, where the only remaining peatlands are in Alaska. For the other Marine Isotope Stage (MIS) 3 time periods, the peat area is similar to the LGM as the ice area prescribed (based on ICE-5G) is similar (though its peak height is substantially lower), but as sea-

CPD
9, 3519–3561, 2013

level is higher, the total area in some coastal regions of the model is smaller than at the LGM.

Sphagnum spores and peat basal dates both indicate southwards expansions of peatlands into the American Midwest and the East coast of the USA during the deglaciation between 16–12 kyr (Halsey et al., 2000; MacDonald et al., 2006). In Europe there is less direct pollen or core-based evidence during the deglaciation, but van Huissteden (2004) presents some evidence for the expansion of peat layers in Northern Europe during MIS 3, also a time period of abrupt shifts in atmospheric CH_4. As sensitivity tests, we considered two extra scenarios for each palaeo time period. The first is the complete removal of the Siberian peat complex in order to match the model peat map to the late glacial distribution of Yu et al. (2010). The second involves introducing new peat gridcells in North America and Europe. Over North America, 0.35×10^6 km^2 (equivalent to 35 % of the modern distribution for North America) of peatland was prescribed in the area South West and East the Great Lakes consistent with the areal estimate of Halsey et al. (2000) (their Fig. 8), whilst a similar area of peatland was added in Northern Europe for comparison.

CH_4 fluxes simulated by LPJ-WHyMe must be corrected for the overestimate of modern observed peatland area prescribed in the model, as well as for the effect of microtopography which is not explicitly modelled (Spahni et al., 2011). The latter correction takes the value of 0.75, whilst the areal correction factor used here is 0.30 (c.f. 0.38 in Spahni et al., 2011), giving a total peatland area in the pre-industrial of 3.20×10^6 km^2

In this work for comparison purposes we also make use of the SDGVM (Sheffield Dynamic Global Vegetation Model Woodward et al., 1995; Beerling and Woodward, 2001) which includes a generalized wetland CH_4 model (e.g. Valdes et al., 2005; Singarayer et al., 2011). SDGVM uses upland PFTs to represent the carbon cycling in wetlands, includes nitrogen cycling of both above- and below- ground stores and incorporates 8 soil carbon pools. In this generalized scheme, the different pathways of CH_4 transport from the soil to the atmosphere are not treated separately and though emissions are not allowed when the temperatures reach freezing, SDGVM does not currently

CPD
9, 3519–3561, 2013

include the impact of freezing of soil water on plant water availability. The potential wetland area is calculated from the simulated soil moisture in SDGVM and emissions are calculated on monthly basis as a function of soil respiration, surface temperature, water table depth and sub-grid orography. SDGVM emissions are corrected to give the same pre-industrial total of 147 Tg CH_4 yr^{-1}, the value used in atmospheric chemistry simulations by Valdes et al. (2005); Levine et al. (2011). This also means that the pre-industrial Northern extra-tropical flux (≥45° N) is very similar in SDGVM and LPJ-WHyMe. SDGVM and LPJ-WHyMe are very different in terms of processes resolved, and show different levels of sensitivity of CH_4 emissions to environmental factors (e.g. Wania et al., 2013; Melton et al., 2013). The major differences between the two models are summarised in Table 2.

3 Results

The palaeoclimate GCM simulations are summarised in Table 1 and compared with temperature anomalies derived from ice-core temperature reconstructions. FAMOUS shows more extreme cooling during the LGM and MIS3 time periods than equivalent simulations with HadCM3 (Singarayer and Valdes, 2010). For example, the cooling at the LGM relative to the pre-industrial is 20 °C in FAMOUS, compared to around 14 °C in HadCM3.

The changes in AMOC which are the principal drivers of the simulated abrupt change are shown for the 3 phases of each simulation in Fig. 1. The non-forced phase (with no prescribed freshwater input) of each simulation is denoted EQ, whilst the cold and warm phases are denoted HS (Heinrich stadial) and GI (Greenland Interstadial) respectively. These definitions are applied loosely since the climatic forcings which cause the oscillations observed in ice-core data are unknown. The model EQ AMOC values are relatively stable across the different time-periods at around 20 Sv (1 Sv = 10^6 m^3 s^{-1}) which is close to the pre-industrial value of 18 Sv. The large changes in AMOC forced by freshwater input are also similar amongst the different sim-

CPD
9, 3519–3561, 2013

ulations, especially when considering the considerable interannual variability as shown by the vertical bars. The only exception is the ±1.0 Sv LGM simulation for which the HS AMOC value is weaker than the corresponding HS phases in the remaining simulations. In the 0.5 Sv simulations, the AMOC varies between an average HS value of around 5Sv and a GI value of 35 Sv.

The pattern of GI-HS warming is shown in Fig. 2 for the annual mean for 4 of the simulations. The patterns in the remaining time-periods are similar to those of the 38 kyr model and are not shown. In all cases there is a clear contrast between the land and ocean response, with a larger signal over ocean. Over Eurasia the warming is generally stronger than over North America, although this difference is minimal in the summer mean (not shown). The differences between the 0.5 Sv simulations (LGM, 14 and 38 kyr) are relatively small, indicating a reasonably low sensitivity to the different boundary conditions imposed, such as the lower ice-sheets or atmospheric CO_2. FAMOUS does show more sensitivity to the magnitude of freshwater forcing, as the ±1.0 Sv LGM simulation shows amplified temperature changes, particularly over the North Atlantic and Europe.

The abrupt changes over Greenland are also compared with reconstructions derived from ice-cores in Table 1. In the model (averaged over 60–20° W, 70–80° N) the total warming (GI-HS) ranges from 7.3 to 9.4 °C which is at the lower end of the estimates of Greenland warming, see column 3, Table 1. The model temperature anomaly averaged over a box located further southwards displays a larger magnitude. For example over the range 60–80° N by 60–20° W, the maximum warming is 11.1 °C. This implies that, were the model to simulate a more Northwards penetration of the oceanic heat transport, the temperature signal over Greenland may be in better agreement with the changes inferred from Greenland ice-cores, but other processes missing in this idealistic freshwater forcing scenario could also be important.

Equivalent precipitation anomalies are shown in Fig. 3, where the asymmetric response between North America and Eurasia is also seen. Generally the signal is again stronger over the ocean. The precipitation changes in all seasons are minimal over

CPD
9, 3519–3561, 2013

North America, and for coastal gridcells show a drying, which is opposite of the small increases in precipitation simulated over much of Western Eurasia.

3.1 Comparison of climate anomalies with reconstructions

A variety of proxy data record abrupt glacial climate change from across the northern hemisphere and could serve as indicators of potential mechanisms. Speleothems from China (Wang et al., 2001) show strong correlation with millennial variability of Greenland ice-cores, suggesting more intense summer monsoons in China during Greenland interstadial phases. Global pollen records of sufficient temporal resolution are relatively sparse but have been collated globally for important D-O events (Harrison and Sanchez-Goñi, 2010). For the transition during D-O 8 these records indicate significant increases in temperature in Europe and eastern North America, whilst significant changes to plant available moisture occur mainly in Europe, with a more complex pattern of both increases and decreases over tropical South America. Changes in the inter-tropical convergence zone (ITCZ) precipitation are also inferred for the Cariaco basin which located at 10° N on the coast of central America (Peterson et al., 2000).

The abrupt transitions in these simulations lead to large changes in annual and especially winter temperatures and precipitation over Europe and the North Atlantic. There is also a concurrent southwards shift in the ITCZ during the HS phase similar to previous modelling studies. There is no Northwards shift of ITCZ in the GI relative to the EQ phase (Hopcroft et al., 2011). There is no significant change in the Asian monsoon in contrast to the speleothem reconstructions, but there is a strong decrease in the strength of the summer Indian monsoon system during the cool HS phase. This is similar to the results of Pausata et al. (2011). There is no significant change in the Indian or Asian Monsoons in the warm GI phase relative to the unperturbed EQ phase. The precipitation anomaly pattern over South America is complex and shows increases over the Northern part of the continent with a strong decrease over the Atlantic coastal areas. This is broadly consistent with opposing signals inferred from speleothem at locations 10° S and 11° N (Kanner et al., 2012; Peterson et al., 2000, respectively), but

CPD
9, 3519–3561, 2013

the pattern of changes is not in particularly good agreement with inferences from pollen data (Harrison and Sanchez-Goñi, 2010) for D-O event 8.

Gherardi et al. (2005) inferred approximately 10 °C increase in SST during the Bølling-Allerød at a site in the Western Atlantic at 37° N. This is comparable with the modelled annual mean GI-HS warming in the 14kyr simulation in this region. Elliot et al. (2002) reconstructed 7 °C and 3.5 °C summer SST warming at a site in the Western Atlantic at 55N for the Bølling-Allerød and D-O 8 respectively. The former is consistent with the model simulations, although the annual mean warming at this location is much larger in the model, but the latter is much smaller than simulated for the 38 kyr event. Further North at site SO82-5 (59° N) van Kreveld et al. (2000) inferred oscillations of 4 °C which is around a factor of 4 smaller than the changes simulated in the model in any time period. Other SST estimates of both winter and summer change for D-O 8 are summarised by Harrison and Sanchez-Goñi (2010) and show SST increases of 8–10 °C in both seasons for sites at latitude 37–45° N in the Atlantic. These changes are consistent with the modelled change in summer, but the winter temperature change is larger in the model which is in places larger than 15 °C. The model fails to reproduce the 3-5 °C warming over the Santa Barbara basin inferred by Hendy and Kennett (2000).

3.2 CH_4 emissions in each time period

The prescribed extra-tropical peatland area for the LGM is 2.2×10^6 km^2, with similar values for the remaining time periods as summarised in Table 3. The base EQ emissions in LPJ-WHyMe in the time periods considered vary between 33.6 Tg CH_4 yr^{-1} in the pre-industrial to only 1.9 Tg CH_4 yr^{-1} at the LGM as shown in Fig. 5 and summarised in Table 3. For comparison when forced with CRU 1961–1990 climatology regridded to FAMOUS resolution, the Boreal (> 45° N) peatland source is 31.0 Tg CH_4 yr^{-1}. Both of these values are similar to the range of 38.5–51.1 Tg CH_4 yr^{-1} simulated by Spahni et al. (2011), and are within the range of inverse estimates of 33 ± 18 Tg CH_4 yr^{-1} (Chen and Prinn, 2006).

CPD
9, 3519–3561, 2013

The LGM value reduces to 0.9 Tg CH_4 yr^{-1} when the Siberian peatlands are removed. The baseline rates at 38 and 14 kyr are intermediate at 4.9 and 11.1 Tg CH_4 yr^{-1} respectively, and these reduce to 1.2 and 4.0 Tg CH_4 yr^{-1} without Asian sources. The warmer climate and higher CO_2 level at 14kyr stimulate the Asian peatlands so that emissions are higher than during the 38 kyr climate, despite similar orbital insolation patterns at Northern latitudes. The comparisons with the LGM and baseline 38 kyr emissions rates inferred by Fischer et al. (2008) and Bock et al. (2010) respectively, suggest that with no Siberian peatlands the model emissions are too low in both the LGM and 38 kyr EQ phases, whilst the simulations with extra peat areas are slightly too high. This is perhaps surprising since these ice-core inferred sources are for northern regions rather than peatlands only. The new interpolar gradient data of Baumgartner et al. (2012) show that the northern emissions estimates of Fischer et al. (2008) and Bock et al. (2010) are indeed too low. The inferred northern (3-box model) LGM source of (Baumgartner et al., 2012) is around half the late Holocene value. Whilst the LPJ-WHyMe results show a very strong reduction in the peatland emissions, this peatland source is not directly comparable with the northern source inferred from the interpolar CH_4 gradient which additionally includes sub-tropical regions.

3.3 Transient CH_4 emissions in LPJ-WHyMe

The peatland emissions respond relatively strongly to the transient changes in climate induced by the freshwater perturbation. The transient decadally averaged CH_4 emissions in LPJ-WHyMe are shown together in Fig. 6. The marked response is especially evident in the 14 kyr simulation, where although the fractional increase in emissions is only 36 % during the warm (GI) phase relative to the unforced (EQ) initial stage, the absolute change is 4 Tg, larger than the increases during the other time periods which are 1.6 and 1.0 Tg yr^{-1} in the LGM and 38 kyr simulations respectively. The magnitude of the transition from GI-HS, i.e. the largest change in each simulation ranges from is 2.8 to 7.5 Tg CH_4 yr^{-1} in the LGM and 14 kyr simulations respectively. The spatial pat-

CPD
9, 3519–3561, 2013

tern of GI-HS emission anomalies is shown for these two simulations in Figs. 7 and 8. The largest anomalies are seen over Europe, with the magnitude of change decreasing with latitude. The GI-HS change in the 14 kyr simulation shows a similar feature but a larger area of significant emissions anomalies.

Removing the peat area in Siberia (as shown in Fig. 4) reduces the EQ emission rates by more than 50 % in each time period. Consequently the abrupt reponse (GI-HS) is also reduced, but by less than 50 %. Prescribing extra areas of peat near the North Atlantic in Europe and North America results in a significant increase in emissions. In the 14 kyr simulation, the EQ emissions increases from 11.1 to 21.1 Tg CH_4 yr^{-1} and in the 38 kyr simulation from 4.9 to 14.4 Tg CH_4 yr^{-1}. Similarly the GI-HS response is larger, giving abrupt changes that range from 7.7 to 9.4 Tg CH_4 yr^{-1} in the 60 and 38 kyr simulations respectively.

4 Analysis

4.1 Comparison with the ice-core inferences

The two earlier studies of Fischer et al. (2008) and Bock et al. (2010) estimated changes in Boreal sources during the deglaciation and D-O events 7 and 8 using a multi-box model and the ice-core interpolar gradient and measured changes in the δD of CH_4. The box model of Bock et al. (2010) requires an increase in the Boreal source from 6 to 30 Tg CH_4 yr^{-1} during the initial rapid phase of the D-O event 8 (their SOM Table 2). For the larger change in atmospheric CH_4 (increase of 160 ppbv) during the Bølling-Allerød (14kyr) the Boreal source is inferred by Fischer et al. (2008) (see their SOM) to have increased to approximately 36 Tg CH_4 yr^{-1}. The more recent interpolar gradient data from Baumgartner et al. (2012) (from NGRIP and EDML) and prior work of Brook et al. (2000) based on GISP2 and Taylor Dome ice-cores, both suggest more modest increases at high latitudes, with a more important contribution from sub-tropical and northern tropical regions.

CPD
9, 3519–3561, 2013

Comparing the LPJ-WHyMe changes in CH_4 emissions across all of the simulations summarised in Table 3 it is clear that none of the simulated changes are near to the values required by the ice-core constraints of Bock et al. (2010). The largest signal occurs in the 38 kyr simulation when the extra NA + EU peat areas are prescribed, and yet this increase is only 40 % of the value required. The change for the equivalent LGM simulation is 8.4 Tg, and is similarly large because although the temperatures are lower, some of the land areas submerged at 38 kyr, are fully exposed at the LGM, increasing the areas of peatland in Europe and eastern North America.

If peatlands can indeed expand rapidly (as suggested by MacDonald et al., 2006), then changes in the emitting area may be an important consideration for the CH_4 budget during D-O events. Assuming the same climate sensitivity of an expanding peat area as that already included in the model, for the 38 kyr (no Sib + EU + NA) simulation the extra peatland area required during the abrupt warming would amount to more than a doubling (×2.2). Thus even for the simulation with the highest climate sensitivity (namely additional peatland is prescribed in the North Atlantic region) the change in total peatland area required to satisfy the conclusions of Bock et al. (2010) appears large when considering the timescale of CH_4 change which is of the order of 25–100 yr (Huber et al., 2006). This highlights the low magnitude of simulated CH_4 emission increases in comparison with the overall measured changes in atmospheric CH_4 during these abrupt events.

4.2 Comparison with SDGVM

Comparisons are now made between the results from the peatland model LPJ-WHyMe and a wetland model in SDGVM. This should give information on processes important for abrupt CH_4 change and provide some insight into the uncertainty associated with the simulated CH_4 fluxes. The summary values for all of the simulations are shown for comparison with LPJ-WHyMe in Table 4, which shows that SDGVM predicts a much larger area of emissions than any of the prescribed areas used in LPJ-WHyMe. The LGM emissions in SDGVM are also larger than in LPJ-WHyMe. The reductions of emis-

CPD
9, 3519–3561, 2013

sions at the LGM are 94 and 65 % in LPJ-WHyMe and SDGVM respectively, showing that LPJ-WHyMe is much more sensitive to the LGM low CO_2 and climate conditions. The influence of the lowered atmospheric CO_2 versus the LGM climate can be assessed by running both models forced with LGM climatology, but pre-industrial CO_2 levels. Doing so demonstrates that 88 % of the LGM reduction in emissions is due to climate, with only the 12 % as a result of the prescribed reduction in atmospheric CO_2 concentration.

The GI-HS transition for the LGM is 5.4 Tg CH_4 yr^{-1} in SDGVM and the spatial pattern of GI-HS is shown in comparison with LPJ-WHyMe in Fig. 7. In SDGVM for the Boreal region, the wetland area decreases during the cooling (HS) and increases during the warming (GI), but the fractional changes are small, and the majority of the change in emissions is a consequence of climatic influence on emission rates rather than changes in the simulated wetland area.

LPJ-WHyMe appears to be more sensitive to the imposed climate, since the proportional changes are larger. For example, in the LGM simulations the GI-HS change is 153 % of the control LGM value, compared to only 40 % in SDGVM. This may be because the spatial distribution of wetlands is different, or due to other internal processes in the model. We explored this aspect more robustly by configuring a modified version of SDGVM, here denoted SDGVM-LPJ-h, only for peatland grid-cells prescribed in LPJ-WHyMe (in the default configuration). Three other modifications were introduced to SDGVM-LPJ-h in order to minimise differences between the two models: (i) the water-table depth values calculated by LPJ-WHyMe were used instead of those calculated using the SDGVM soil moisture content, (ii) the Q_{10} of CH_4 production sensitivity to temperature was increased from 1.5 to 2.0 and (iii) the orographic correction applied in SDGVM to modify the wetland area and flux was removed. The output of this model then has the same spatial distribution of wetlands as the equivalent LPJ-WHyMe simulation, the water table position will implicitly include the effect of soil freezing (from LPJ-WHyMe), whilst the carbon substrate available for methanogenesis (which is still calculated within SDGVM) does not. The total pre-industrial emissions of SDGVM-LPJ-

CPD
9, 3519–3561, 2013

h are scaled to match those of LPJ-WHyMe so that differences between the models are more easily quantified.

The emissions in each simulation are compared in Table 4. The LGM drop in SDGVM-LPJ-h is only 60 % compared with 95 % in LPJ-WHyMe showing that the latter remains more sensitive to the imposed climate anomalies. Further the GI-HS fluctuation in LPJ-WHyMe is still relatively larger than in SDGVM-LPJ-h at 147 % compared with only 36 % in SDGVM-LPJ-h which is actually lower than the value in SDGVM alone (40 %). This is the result of the different areal extension of wetlands used in the original and hybrid SDGVM versions, specifically the contributions of the larger area of circum-Atlantic wetlands (where the climate anomalies are larger) in the original model version.

In order to further understand these differences the net primary productivity (NPP) averaged over the prescribed peatland gridpoints were compared. Whilst both models show a similar PI value of around 2.5 GtC yr^{-1}, SDGVM shows a much smaller change in NPP at the LGM, with a reduction of around 50 % compared to 90 % in LPJ-WHyMe. This could be a result of the inclusion of the nitrogen cycle in SDGVM or due to differences in the sensitivities of the plant functional types in the two models. This low sensitivity is not evident in transient anomaly time-series for the abrupt climate events, for which the absolute changes in NPP in the two models are very similar at around ±0.2 GtC yr^{-1} for the HS and GI phases. The relatively large reduction in NPP simulated by LPJ-WHyMe is much greater especially in the colder climates such as the LGM and 38 kyr than in SDGVM. This is because the initial EQ values are lower than in the corresponding SDGVM simulation. Using NPP to predict CH_4 emissions in the different time periods as a linear function of the ratio of NPP (Whiting and Chanton, 1993) in that time period relative to the pre-industrial, we find that this over-predicts emissions in LPJ-WHyMe by up to 89 % but the maximum error is only ±15 % for SDGVM. This implies that the climate sensitivity of LPJ-WHyMe additionally derives from the processes involved in emissions and transport of CH_4 that are not represented in SDGVM.

CPD
9, 3519–3561, 2013

Taking the same approach for the abrupt transition from HS to GI is less informative as the different carbon stocks, respiration rates and NPP are unlikely to be in equilibrium during the abrupt climate changes. Instead, a further model hybrid is tested in which the SDGVM-LPJ-h now reads the monthly heterotrophic soil respiration H_r from LPJ-WHyMe . This version is called SDGVM-LPJ-hR_h. SDGVM-LPJ-hR_h includes both the soil moisture and water table depth and the carbon substrate from LPJ-WHyMe , but still lacks a representation of the processes related to CH_4 transport and oxidation through the soil column, or any direct influence due to the position of the active layer depth.

Again emissions are compared for this model version with the previous 3 models in Table 4. This model shows emissions much closer to those of LPJ-WHyMe. In particular the reduction in emissions at the LGM relative to the pre-industrial is now 89 % which compares favourably with 94 % in LPJ-WHyMe, and is much larger than the value of only 61 % in SDGVM-LPJ-h. This also supports the scaling of NPP to calculate the EQ emission rates in different time periods. However, this model version (SDGVM-LPJ-hR_h) still considerably underestimates the transient emission changes seen in LPJ-WHyMe. For example in the LGM simulation the increase during the GI relative to the EQ is 84 % in LPJ-WHyMe, but only 33 % in SDGVM-LPJ-hR_h, though this is far larger than the 10 % in SDGVM-LPJ-h. The values for the warmest simulation (14 kyr) follow a similar pattern: 36 % for LPJ-WHyMe versus 18 % in SDGVM-LPJ-hR_h and 12 % in SDGVM-LPJ-h. Thus whilst the long-term equilibrium (EQ) values can be reconciled by taking the carbon substrate from LPJ-WHyMe in this hybrid model setup, the transient sensitivity of LPJ-WHyMe cannot.

A final model version SDGVM-LPJ-hR_hT now takes the 25cm soil temperature predicted by LPJ-WHyMe in the SDGVM-LPJ-hR_h model rather than using the surface air temperature simulated by FAMOUS. The 25cm soil temperature is chosen because it controls the rates of heterotrophic respiration within LPJ-WHyMe for CH_4 emissions (Wania et al., 2010). The LGM reduction in emissions in SDGVM-LPJ-hR_hT is 94 %, comparable to 95 % in LPJ-WHyMe, and the transient sensitivity is approximately the

CPD
9, 3519–3561, 2013

same in SDGVM-LPJ-hR_hT and LPJ-WHyMe (as shown in Table 4). This suggests that the effects of soil freezing and the position of the active layer depth increase the sensitivity of the CH_4 emissions in cold regions and that only by including this can we reconcile the magnitude of change in CH_4 emissions seen in LPJ-WHyMe with the hybrid model considered here. Other differences remain, particularly in the remaining time periods and these must be related to other differences between LPJ-WHyMe and SDGVM not considered in the above analysis.

4.3 Concentration predictions

The modelled changes in emissions between the cold and warm states (HS and GI) are now used to calculate the likely change in atmospheric CH_4. This allows direct comparison with the ice-core record for all events simulated without the complications arising from deconvolving the emissions estimates from the interpolar gradient. Numerical simulations of the major influences on the atmospheric CH_4 lifetime during a glacial abrupt warming event suggest that the lifetime may be relatively constant (Levine et al., 2012). Thus we employed a constant lifetime of 8.6 yr (following prior work: Hopcroft et al., 2011) and assumed a uniform conversion of emissions to atmospheric concentration of 2.75 ppbv Tg^{-1}. The results are increased by 10 % to account for the self feedback of CH_4 on its own lifetime, based on analysis of glacial atmospheric chemistry simulations (Levine et al., 2011). The SDGVM total pre-industrial emissions are scaled to match the value of 147 Tg CH_4 yr^{-1} used by Valdes et al. (2005) and Levine et al. (2011) in order to be more consistent with previous calculations of atmospheric concentration changes for glacial time periods. This means that the total concentration predictions are slightly smaller than those predicted in previous work (Hopcroft et al., 2011). The LPJ-WHyMe values are given as differences with the emissions from SDGVM over the equivalent area, to illustrate the effect of the inclusion of more complex model dynamics. Two LPJ-WHyMe scenarios are considered. The standard case and that with extra peatland prescribed in North America and Europe. To avoid double counting in the latter case, the SDGVM emissions are only summed over gridcells

CPD
9, 3519–3561, 2013

below 45° N which do not contain prescribed peatlands in the equivalent LPJ-WHyMe scenario.

The maximum calculated change in atmospheric CH_4 calculated by summing SDGVM (<45° N) and LPJ-WHyMe (≥45° N) is 102 ppbv in the 14 kyr case, whilst the maximum total change is only 86 and 95 ppbv in the 60 and 44 kyr cases respectively. Depending on the area of peat prescribed, the LPJ-WHyMe model can simulate both less and more change than in SDGVM, with the exception of the 14kyr case. The predicted CH_4 changes are compared against ice-core data in Table 1. The SDGVM results underestimate the events by between 23–57 %. Inclusion of LPJ-WHyMe only improves the agreement with ice-core data when the maximum peat area simulations are used in the LGM, 44 and 60 kyr simulations. In these simulations LPJ-WHyMe increases the change by up to 10 %. Despite the increased transient sensitivity of the LPJ-WHyMe model, the results still suggest underestimation of the observed rapid CH_4 increases. This is partly because LPJ-WHyMe predicts lower initial (EQ) emissions than SDGVM during each time period.

The significant variation in the amplitude of the abrupt CH_4 changes as evident from the ice-core data (Flückiger et al., 2004; Huber et al., 2006) does not appear to be well replicated in the simulations. For example, the CH_4 change at D-O event 17 is 65 % larger than for event 11. Singarayer et al. (2011) demonstrated that the SDGVM model is able to replicate the orbital timescale changes in CH_4 emissions rather well. Hence the lack of variability in the size of the abrupt changes simulated here could result from some feature of the physical climatic forcing. For example, the abrupt changes in the AMOC are very similar in the different time periods considered.

5 Discussion

We have performed a series of transient coupled GCM simulations of five time periods considered important for Dansgaard-Oeschger events of the last glacial period. Using freshwater forcing to perturb the model AMOC, we instigate rapid warming in the

CPD
9, 3519–3561, 2013

North Atlantic region, mostly as a result of increased heat transport from the resurgent AMOC, but also partly deriving from feedbacks from sea-ice cover and atmospheric heat transport. The warming over Greenland in the model is of the order of 8–9 °C which is at the lower end of the ice-core reconstructions. Doubling, the magnitude of the freshwater forcing (which equates to 10 m/century sea-level rise) does not reproduce the largest magnitude of warming observed in Greenland of up to 16 °C (Huber et al., 2006; Wolff et al., 2010).

The inferred source changes for northern sources from recent data of Baumgartner et al. (2012) (in agreement with inferences of Brook et al. (2000)) suggest that northern sources were approximately halved during the last glacial period. The strong reduction in northern peatland emissions in LPJ-WHyMe is consistent with this inference, but it is not possible to differentiate between the boreal and sub-tropical northern sources using the ice-core interpolar gradient and so quantitative comparison between LPJ-WHyMe and the ice-core-based inference is difficult.

Using the transient monthly-mean GCM outputs, we have forced a series of simulations of the LPJ-WHyMe peatland and CH_4 emissions models. Comparisons with inferences drawn from the ice-core derived inter-hemispheric gradient and δDCH_4 of CH_4 Bock et al. (2010) indicate that the model simulations significantly under-predict the abrupt changes in emissions, but this is in agreement with the newer lower values for the glacial and interstadial interpolar gradient (Baumgartner et al., 2012). Simple calculations of the atmospheric concentration changes in response to global emission increases also under-predict the measured changes from ice-cores.

Comparison of the results with an independent DGVM (SDGVM) suggests that the model complexity of LPJ-WHyMe leads to increased sensitivity, although there are major structural differences between the models analysed which hinders quantitative conclusions. Three modified version of SDGVM in which the CH_4 module is forced with hydrological values, soil respiration and soil temperature variables from LPJ-WHyMe were configured in order to enable a more quantitative comparison. For the abrupt warming relative to the EQ, LPJ-WHyMe was, in terms of CH_4 emissions, up to 8 times

CPD
9, 3519–3561, 2013

more sensitive than the SDGVM-LPJ-h model and up to 4 times more sensitive than the SDGVM-LPJ-hR_h model. This analysis indicated that the carbon substrate in LPJ-WHyMe is more sensitive to the imposed climate, most likely due to the influence of soil freezing on plant moisture availability, whilst hydrological differences between LPJ-WHyMe and SDGVM were less important. Inclusion of the influence of soil freezing on the carbon substrate supply (by taking heterotrophic respiration from LPJ-WHyMe in the SDGVM-LPJ-hR_h model) was mostly able to reproduce the base (EQ) emissions in different time periods. However, it appears that the inclusion of vertically resolved emission, transport and oxidation of CH_4, and their dependence on the active layer depth is crucial for fully resolving the magnitude of the transient changes in emissions in these simulations.

A weak CH_4 response to abrupt AMOC variations has also been found in prior work using SDGVM and ORCHIDEE models forced with FAMOUS climate output (Hopcroft et al., 2011; Ringeval et al., 2013), and in a newer version of LPJ-WHyMe forced with a freshwater scenario under modern climatic conditions using a different model, CCSM1.4 (Zürcher et al., 2013). A recent model intercomparison (Melton et al., 2013) quantified the sensitivities of 10 CH_4 emissions models including LPJ-WHyMe, SDGVM and ORCHIDEE. This showed that current models span a range of sensitivities to temperature, precipitation and atmospheric CO_2. Examining the extra-tropical response to a uniform temperature and precipitation increase of 3.4 °C and 3.9 % respecitively, these three models span the range from −26 to +24 % change in response to warming (ORCHIDEE and LPJ-WHyMe respectively) and from 3 to 10 % change in response to precipitation increase (SDGVM and ORCHIDEE respectively). Together this suggests that the main conclusions reached here may be robust, but that inter-model differences are still large and require further investigation.

An important consideration for comparing emissions and concentrations of CH_4 is the change in atmospheric lifetime which is largely controlled by the atmospheric burden of OH. OH concentrations are controlled directly by atmospheric temperatures and mixing and indirectly through the emissions of volatile organic compounds from

CPD
9, 3519–3561, 2013

vegetation. Two recent studies with 3-D atmospheric chemistry-transport simulations suggested that the combined impact of these two effects leads to a negligible change in CH_4 lifetime both for the G-IG transition and for abrupt climate events (Levine et al., 2011, 2012).

Other potentially relevant CH_4 sources not addressed in this work include biomass burning, thaw lakes and the oceans. Whilst records of charcoal suggest a dynamic relationship between climate and biomass burning (Daniau et al., 2010), ice-core isotopic evidence appears to argue against substantial contributions on either the glacial-inter glacial (Fischer et al., 2008) or abrupt time-scales (Bock et al., 2010). Thaw lakes are a large source of uncertainty as they are difficult to represent realistically in global-scale models. Controversy remains over whether geological evidence signifies a rapid expansion of thaw lakes during the abrupt CH_4 increase at the end of the Younger-Dryas (Walter et al., 2007; Reyes and Cooke, 2011) and further work is required to establish the magnitude and sensitivity of thaw lake emissions under atmospheric warming scenarios. Evidence for methanogenic bacterial communities in sub-glacial environments suggests a sub-glacial source of CH_4 (Wadham et al., 2008). The potential influence of subglacial environments on atmospheric CH_4 or on carbon substrate supply subsequent to deglaciation is uncertain.

A primary limitation in the current study is the prescription of peatland areas within the LPJ-WHyMe model. We have attempted to address this uncertainty by analysing the signals from 4 different distributions for each time period, but stronger palaeo-time constraints on peatland areas would be invaluable. Another approach could rely on reconstructions of ice-sheet areas through time, adding peat areas as a function of time since deglaciation. Information on the area of glaciation for times prior to the Last Glacial Maximum is very limited due to the destruction of landscape markers by the expanding ice sheets. An alternative approach would involve predicting the accumulation of peat as a function of environmental controls (e.g. Frolking et al., 2010; Kleinen et al., 2012).

CPD
9, 3519–3561, 2013

6 Conclusions

Results from these simulations with a coupled atmosphere-ocean GCM and two ecosystem CH_4 emissions models (SDGVM and LPJ-WHyMe) suggest that changes in the Atlantic MOC are unable to fully explain abrupt changes in atmospheric CH_4 as reconstructed from ice-cores. The weak peatland source changes are consistent with new interpolar gradient but the total emissions increases underestimate the measured changes in atmospheric concentration. Relative to a more generalized wetland scheme (such as SDGVM), the inclusion of peatland and permafrost processes in the LPJ-WHyMe model increases the climatic sensitivity of CH_4 emissions. This increased sensitivity in the peatland model under equilibrium conditions is mostly due to differences in the carbon cycle productivity, whilst the increased sensitivity to abrupt warming is also partly due to the effects of freezing on soil thermodynamics. The higher sensitivity in LPJ-WHyMe however implies low simulated baseline emissions in each of the glacial time periods. This means that the rapid changes in CH_4 emissions are of similar magnitude in the peatland model as in the generalized wetland scheme. The variability in the magnitude of the abrupt CH_4 rises inferred from the ice-core record is also not convincingly replicated in the model, and this could be related to some feature of the climate scenarios used.

The CH_4 changes during D-O events are extremely large when compared with natural contemporary variations, and thus constitute important targets for improved understanding of the global CH_4 cycle. Changes in wetland emissions during these events have been inferred to be relatively strong and modelling efforts should focus on how different weltand process representations (Ringeval et al., 2013) and mechanisms of climate change might be important for understanding D-O events. Recent studies have highlighted potential alternative mechanisms for abrupt warming aside from changes in the AMOC (Seager and Battisti, 2007; Clement and Peterson, 2008; Petersen et al., 2013), but relatively few of these have been pursued in appropriate climate modelling frameworks (Wunsch, 2006; Seager and Battisti, 2007). Future research could seek to

CPD
9, 3519–3561, 2013

diversify beyond freshwater the range of perturbations imposed on coupled GCMs in this context, particularly as this could lead to different patterns of climate change and hence CH_4 emissions.

Acknowledgements. This work was funded by the joint UK and France QUEST-INSU DESIRE (Dynamics of the Earth System and the Ice-core Record) project, and partly by a NERC UK grant Earth System Modelling of Abrupt Climate Change. We thank James Levine, Bruno Ringeval and Eric Wolff for discussions on many aspects of the CH_4 cycle and abrupt climate change. This work was carried out using the computational facilities of the Advanced Computing Research Centre, University of Bristol – http://www.bris.ac.uk/acrc/.

References

Baumgartner, M., Schilt, A., Eicher, O., Schmitt, J., Schwander, J., Spahni, R., Fischer, H., and Stocker, T. F.: High-resolution interpolar difference of atmospheric methane around the Last Glacial Maximum, Biogeosciences, 9, 3961–3977, doi:10.5194/bg-9-3961-2012, 2012. 3521, 3531, 3532, 3539

Beerling, D. J. and Woodward, F. I.: Vegetation and the Terrestrial Carbon Cycle: Modelling the first 400 Million Years, Cambridge: Cambridge University Press, 2001. 3522, 3526

Berger, A. and Loutre, M.: Insolation values for the climate of the last 10 million years, Quaternary Sci. Rev., 10, 297–317, 1991. 3523

Blunier, T. and Brook, E.: Timing of Millennial-Scale Climate Change in Antarctica and Greenland During the Last Glacial Period, Science, 291, 109–112, 2001. 3550

Bock, M., Schmitt, J., Moller, L., Spahni, R., Blunier, T., and Fischer, H.: Hydrogen Isotopes Preclude Marine Hydrate CH_4 Emissions at the Onset of Dansgaard-Oeschger Events, Science, 328, 1686–1689, 2010. 3531, 3532, 3533, 3539, 3541

Brook, E. J., Harder, S., Severinghaus, J., Steig, E. J., and Sucher, C. M.: On the origin and timing of rapid changes in atmospheric methane during the last glacial period, Global Biogeochem. Cy., 14, 559–572, 2000. 3521, 3532, 3539

Cao, M., Marshall, S., and Gregson, K.: Global carbon exchange and methane emissions from natural wetlands: Application of a process-based model, J. Geophys. Res., 101, 14399–14414, 1996. 3522, 3551

Chen, Y.-H. and Prinn, R.: Estimation of atmospheric methane emissions between 1996 and 2001 using a three-dimensional global chemical transport model, J. Geophys. Res., 111, D10307, doi:10.1029/2005JD006058, 2006. 3530, 3552

Clement, A. and Peterson, L.: Mechanisms of Abrupt Climate Change of the Last Glacial Period, Rev. Geophys., 46, RG4002, doi:10.1029/2006RG000204, 2008. 3521, 3542

Dällenbach, A., Blunier, T., Flückiger, J., Stauffer, B., Chappellaz, J., and Raynaud, D.: Changes in the atmospheric CH_4 gradient between Greenland and Antarctica during the Last Glacial and the transition to the Holocene, Geophys. Res. Lett., 27, 1005–1008, 2000. 3521

Daniau, A.-L., Harrison, S., and Bartlein, P.: Fire regimes during the Last Glacial, Quaternary Sci. Rev., 29, 2918–2930, 2010. 3541

Elliot, M., Labeyrie, L., and Duplessy, J.-C.: Changes in North Atlantic deep-water formation associated with the Dansgaard-Oeschger temperature oscillations (60–10 ka), Quaternary Sci. Rev., 21, 1153–1165, doi:10.1016/S0277-3791(01)00137-8, 2002. 3530

Fischer, H., Behrens, M., Bock, M., Richter, U., Schmitt, J., Loulergue, L., Chappellaz, J., Spahni, R., Blunier, T., Leuenberger, M., and Stocker, T. F.: Changing boreal methane sources and constant biomass burning during the last termination, Nature, 452, 864–867, 2008. 3531, 3532, 3541

Flückiger, J., Blunier, T., Stauffer, B., Chappellaz, J., Spahni, R., Kawamura, K., Schwander, J., Stocker, T. F., and Dahl-Jensen, D.: N_2O and CH_4 variations during the last glacial epoch: Insight into global processes, Global Biogeochem. Cy., 18, GB1020, doi:10.1029/2003GB002122, 2004. 3521, 3522, 3538, 3550

Frolking, S., Roulet, N. T., Tuittila, E., Bubier, J. L., Quillet, A., Talbot, J., and Richard, P. J. H.: A new model of Holocene peatland net primary production, decomposition, water balance, and peat accumulation, Earth Syst. Dynam., 1, 1–21, doi:10.5194/esd-1-1-2010, 2010. 3541

Ganopolski, A. and Rahmstorf, S.: Rapid changes of glacial climate simulated in a coupled climate model, Nature, 409, 153–155, 2001. 3521, 3524

Gerten, D., Schaphoff, S., Haberlandt, U., Lucht, W., and Sitch, S.: Terrestrial vegetation and water balance: Hydrological evaluation of a dynamic global vegetation model, J. Hydrology, 286, 249–270, 2004. 3523

Gherardi, J.-M., Labeyrie, L., McManus, J. F., Francois, R., Skinner, L. C., and Cortijo, E.: Evidence from the northeastern atlantic basin for variability in the rate of the meridional overturning circulation through the last deglaciation, Earth Planet. Sci. Letts., 240, 710–723, 2005. 3530

CPD
9, 3519–3561, 2013

Gordon, C., Cooper, C., Senior, C. A., Banks, H., Gregory, J. M., Johns, T. C., Mitchell, J. F. B., and Wood, R. A.: The simulation of sst, sea ice extents and ocean heat transports in a version of the Hadley Centre coupled model without flux adjustments, Clim. Dynam., 16, 147–168, 2000. 3523

Granberg, G., Grip, H., Ottosson Löfvenius, M., Sundh, I., Svensson, B. H., and Nilsson, M.: A simple model for simulation of water content, soil frost, and soil temperatures in boreal mixed mires, Water Resour. Res., 35, 3771–3782, 1999. 3551

Halsey, L., D. Vitt, and Gignac, L.: phSphagnum-dominated Peatlands in North America Since the Last Glacial Maximum: Their Occurrence and Extent, The Bryologist, 103, 334–352, 2000. 3526

Harrison, S. and Sanchez-Goñi, M.: Global patterns of vegetation response to millennial-scale variability and rapid climate change during the last glacial period, Quaternary Sci. Rev., 29, 21–22, 2957–2980, 2010. 3529, 3530

Hendy, I. and Kennett, J.: Dansgaard-Oeschger cycles and the California Current System: Planktonic foraminiferal response to rapid climate change in Santa Barbara Basin, Ocean Drilling Program hole 893A, Paleoceanography, 15, 30-42, 2000. 3520, 3530

Hopcroft, P., Valdes, P., and Beerling, D.: Simulating idealized Dansgaard-Oeschger events and their potential impacts on the global methane cycle, Quaternary Sci. Rev., 30, 3258–3268, 2011. 3522, 3524, 3529, 3537, 3540, 3550, 3553

Huber, C., Leuenberger, M., Spahni, R., Flückiger, J., Schwander, J., Stocker, T., Johnsen, S., Landais, A., and Jouzel, J.: Isotope calibrated Greenland temperature record over Marine Isotope Stage 3 and its relation to CH_4, Earth Planetary Sci. Letts., 243, 504–519, 2006. 3520, 3521, 3533, 3538, 3539, 3550

Kanner, L. C., Burns, S. J., Cheng, H., and Edwards, R. L.: High-Latitude Forcing of the South American Summer Monsoon During the Last Glacial, Science, 335, 570–573, 2012. 3520, 3529

Kleinen, T., Brovkin, V., and Schuldt, R. J.: A dynamic model of wetland extent and peat accumulation: results for the Holocene, Biogeosciences, 9, 235–248, doi:10.5194/bg-9-235-2012, 2012. 3541

Korhola, A., Ruppel, M., Seppä, H., Väliranta, M., Virtanen, T., and Weckström, J.: The importance of northern peatland expansion to the late-Holocene rise of atmospheric methane, Quaternary Sci. Rev., 29, 611–617, 2009. 3525

CPD
9, 3519–3561, 2013

Levine, J., Wolff, E., Jones, A., Sime, L., Valdes, P., Archibald, A., Carver, G., Warwick, N., and Pyle, J.: Reconciling the changes in atmospheric methane sources and sinks between the Last Glacial Maximum and the pre-industrial era, Geophys. Res. Lett., 38, L23804, doi:10.1029/2011GL049545, 2011. 3527, 3537, 3541

Levine, J., Wolff, E., Hopcroft, P., and Valdes, P.: Controls on the tropospheric oxidising capacity during an idealized Dansgaard-Oeschger event, and their implications for the rapid rises in atmospheric methane during the last glacial period, Geophys. Res. Lett., 39, L12805, doi:10.1029/2012GL051866, 2012. 3537, 3541

Li, C., Battisti, D., and Bitz, C.: Can North Atlantic Sea Ice Anomalies Account for Dansgaard-Oeschger Climate Signals?, J. Climate, 23, 5457–5475, 2010. 3521

Liu, Z., Otto-Bleisner, B., H. F., Brady, E., Tomas, R., Clark, P., Carlson, A., Lynch-Steiglitz, J., Curry, W., Brook, E., Erickson, D., Jacob, R., Kutzbach, J., and Cheng, J.: Transient Simulation of Last Deglaciation with a New Mechanism for Bølling-Allerød Warming, Science, 325, 310–314, 2009. 3521, 3524

MacDonald, G. M., Beilman, D. W., Kremenetski, K. V., Sheng, Y., Smith, L. C., and Velichko, A. A.: Rapid Early Development of Circumarctic Peatlands and Atmospheric CH_4 and CO_2 Variations, Science, 314, 285–288, 2006. 3525, 3526, 3533

Masson-Delmotte, V., Jouzel, J., Landais, A., Stievenard, M., Johnsen, S. J., White, J. W. C., Sveinbjornsdottir, A., and Fuhrer, K.: Deuterium excess reveals millennial and orbital scale fluctuations of Greenland moisture origin, Science, 309, 118–121, 2005. 3550

Melton, J. R., Wania, R., Hodson, E. L., Poulter, B., Ringeval, B., Spahni, R., Bohn, T., Avis, C. A., Beerling, D. J., Chen, G., Eliseev, A. V., Denisov, S. N., Hopcroft, P. O., Lettenmaier, D. P., Riley, W. J., Singarayer, J. S., Subin, Z. M., Tian, H., Zürcher, S., Brovkin, V., van Bodegom, P. M., Kleinen, T., Yu, Z. C., and Kaplan, J. O.: Present state of global wetland extent and wetland methane modelling: conclusions from a model inter-comparison project (WETCHIMP), Biogeosciences, 10, 753–788, doi:10.5194/bg-10-753-2013, 2013. 3527, 3540

Merkel, U., Prange, M., and Schulz, M.: ENSO variability and teleconnections during glacial climates, Quaternary Sci. Rev., 29, 86–100, 2010. 3524

New, M., M. Hulme, and P. D. Jones: Representing twentieth century space-time climate variability. Part 1: Development of a 1961-1990 mean monthly terrestrial climatology, J. Climate, 12, 829–856, 1999. 3525, 3552

NGRIP Project Members: High-resolution record of Northern Hemisphere climate extending into the last interglacial period, Nature, 431, 47–151„ 2004. 3520

CPD
9, 3519–3561, 2013

Pausata, F., Battisti, D., Nisancioglu, K., and Bitz, C.: Chinese stalagmite $\delta^{18}O$ controlled by changes in the Indian monsoon during a simulated Heinrich event, Nat. Geosci., 4, 474–480, 2011. 3529

Peltier, W.: Global glacial isostasy and the surface of the ice age earth: The ICE-5G (VM2) model and GRACE, Annu. Rev. Earth Planet. Sci., 32, 111–149, 2004. 3523, 3525

Petersen, S., Schrag, D., and Clark, P.: A new mechanism for Dansgaard-Oeschger cycles, Paleoceanography, 28, 24–30, 2013. 3521, 3542

Peterson, L. C., Haug, G. H., Hughen, K. A., and Rohl, U.: Rapid changes in the hydrologic cycle of the tropical Atlantic during the last glacial, Science, 290, 1947–1951, 2000. 3520, 3529

Petit, J. R., Jouzel, J., Raynaud, D., Barkov, N. I., Barnola, J.-M., Basile, I., Bender, M., Chappellaz, J., Davis, M., Dalaygue, G., Delmotte, M., Kotlyakov, V. M., Legrand, M., Lipenkov, V. Y., Lorius, C., Pépin, L., Ritz, C., Saltzman, E., and Stievenard, M.: Climate and atmospheric history of the past 420,000 years from the Vostok Ice Core, Antarctica, Nature, 399, 429–436, 1999. 3523

Reyes, A. and Cooke, C.: Northern peatland initiation lagged abrupt increases in deglacial atmospheric CH_4, Proc. Natl. Acad. Sci., 108, 4748–4753, 2011. 3525, 3541

Ringeval, B., Hopcroft, P. O., Valdes, P. J., Ciais, P., Ramstein, G., Dolman, A. J., and Kageyama, M.: Response of methane emissions from wetlands to the Last Glacial Maximum and an idealized Dansgaard-Oeschger climate event: insights from two models of different complexity, Clim. Past, 9, 149–171, doi:10.5194/cp-9-149-2013, 2013. 3540, 3542

Seager, R. and Battisti, D. S.: Challenges to our understanding of the general circulation: abrupt climate change, in: The Global Circulation of the Atmosphere, edited by: Lorenz, E. N., Schneider, T., and Sobel, A. H., Princeton, USA, Princeton University Press, 2007. 3521, 3542

Singarayer, J. and Valdes, P.: High-latitude climate sensitivity to ice-sheet forcing over the last 120 kyr, Quaternary Sci. Rev., 29, 43–55, 2010. 3523, 3527

Singarayer, J., Valdes, P., Friedlingstein, P., Nelson, S., and Beerling, D.: Late Holocene methane rise caused by orbitally controlled increase in tropical sources, Nature, 470, 82–85, 2011. 3522, 3526, 3538

Smith, R. S., Gregory, J. M., and Osprey, A.: A description of the FAMOUS (version XDBUA) climate model and control run, Geosci. Model Dev., 1, 53–68, doi:10.5194/gmd-1-53-2008, 2008. 3522, 3523

CPD
9, 3519–3561, 2013

Spahni, R., Chappellaz, J., Stocker, T. F., Loulergue, L., Hausammann, G., Kawamura, K., Flückiger, J., Schwander, J., Raynaud, D., Masson-Delmotte, V., and Jouzel, J.: Atmospheric methane and nitrous oxide of the late pleistocene from Antarctic ice cores, Science, 310, 1317–1321, 2005. 3521, 3523

Spahni, R., Wania, R., Neef, L., van Weele, M., Pison, I., Bousquet, P., Frankenberg, C., Foster, P. N., Joos, F., Prentice, I. C., and van Velthoven, P.: Constraining global methane emissions and uptake by ecosystems, Biogeosciences, 8, 1643–1665, doi:10.5194/bg-8-1643-2011, 2011. 3526, 3530, 3552

Valdes, P., Beerling, D., and Johnson, C.: The ice age methane budget, Geophys. Res. Lett., 32, L02704, doi:10.1029/2004GL021004, 2005. 3526, 3527, 3537

van Huissteden, J.: Methane emission from northern wetlands in Europe during Oxygen Isotope Stage 3, Quaternary Sci. Rev., 23, 1989–2005, 2004. 3526

van Kreveld, S., Sarnthein, M., Erlenkeuser, H., Grootes, P., Jung, S., Nadeau, M. J., Pflaumann, U., and Voelker, A.: Potential links between surging ice sheets, circulation changes, and the Dansgaard-Oeschger cycles in the Irminger Sea, 60–18 kyr, Paleoceanography, 15, 425–442, 2000. 3530

Wadham, J., Tranter, M., Tulaczyk, S., and Sharp, M.: Subglacial methanogenesis: A potential climatic amplifier?, Global Biogeochem. Cy., 22, GB2021, doi:10.1029/2007GB002951, 2008. 3541

Walter, K. M., Edwards, M. E., Grosse, G., Zimov, S. A., and Chapin III, F. S.: Thermokarst Lakes as a Source of Atmospheric CH_4 During the Last Deglaciation, Science, 318, 633–636, 2007. 3541

Wang, Y. J., Cheng, H., Edwards, R. L., An, Z. S., Wu, J. Y., Shen, C.-C., and Dorale, J. A.: A High-Resolution Absolute-Dated Late Pleistocene Monsoon Record from Hulu Cave, China, Science, 24, 2345–2348, 2001. 3520, 3529

Wania, R., Ross, I., and Prentice, I. C.: Integrating peatlands and permafrost into a dynamic global vegetation model: 1. evaluation and sensitivity of physical land surface processes, Global Biogeochem. Cy., 23, GB3014, doi:10.1029/2008GB003412, 2009a. 3523, 3524, 3525

Wania, R., Ross, I., and Prentice, I. C.: Integrating peatlands and permafrost into a dynamic global vegetation model: 2. evaluation and sensitivity of vegetation and carbon cycle processes, Global Biogeochem. Cy., 23, GB3015, doi:10.1029/2008GB003413, 2009b. 3523, 3524

CPD
9, 3519–3561, 2013

Wania, R., Ross, I., and Prentice, I. C.: Implementation and evaluation of a new methane model within a dynamic global vegetation model: LPJ-WHyMe v1.3.1, Geosci. Model Dev., 3, 565–584, doi:10.5194/gmd-3-565-2010, 2010. 3523, 3524, 3536

Wania, R., Melton, J. R., Hodson, E. L., Poulter, B., Ringeval, B., Spahni, R., Bohn, T., Avis, C. A., Chen, G., Eliseev, A. V., Hopcroft, P. O., Riley, W. J., Subin, Z. M., Tian, H., van Bodegom, P. M., Kleinen, T., Yu, Z. C., Singarayer, J. S., Zürcher, S., Lettenmaier, D. P., Beerling, D. J., Denisov, S. N., Prigent, C., Papa, F., and Kaplan, J. O.: Present state of global wetland extent and wetland methane modelling: methodology of a model inter-comparison project (WETCHIMP), Geosci. Model Dev., 6, 617–641, doi:10.5194/gmd-6-617-2013, 2013. 3527

Whiting, G. and Chanton, J.: Primary production control of methane emission from wetlands, Nature, 364, 794–795, 1993. 3535

Wolff, E. W., Chappellaz, J., Blunier, T., Rasmussen, S. O., and Svensson, A.: Millennial-scale variability during the last glacial: The ice core record, Quaternary Sci. Rev., 29, 2828–2838, 2010. 3520, 3521, 3539, 3550

Woodward, F., Smith, T., and Emanuel, W.: A global land primary productivity and phytogeography model, Global Biogechem. Cy., 9, 471–490, 1995. 3522, 3526

Wunsch, C.: Abrupt climate change: An alternative view, Quaternary Sci. Rev., 65, 191–203, 2006. 3542

Yin, J., Schlesinger, M., Andronova, N., Malyshev, S., and Li, B.: Is a shutdown of the thermohaline circulation irreversible?, J. Geophys. Res., 11, D12104, doi:10.1029/2005JD006562, 2006. 3521

Yu, Z., Loisel, J., Brosseau, D., and Beilman, D.: Global peatland dynamics since the Last Glacial Maximum, Geophys. Res. Lett., 37, L13402, doi:10.1029/2010GL043584, 2010. 3525, 3526, 3552

Zürcher, S., Spahni, R., Joos, F., Steinacher, M., and Fischer, H.: Impact of an abrupt cooling event on interglacial methane emissions in northern peatlands, Biogeosciences, 10, 1963–1981, doi:10.5194/bg-10-1963-2013, 2013. 3540

CPD
9, 3519–3561, 2013

Table 1. Comparison of GCM and emission model simulations and ice-core data for Greenland (Blunier and Brook, 2001; Flückiger et al., 2004; Masson-Delmotte et al., 2005; Huber et al., 2006; Wolff et al., 2010).

Time	D-O no.	ΔT wrt PI °C	GCM wrt PI °C	ΔT D-O °C	GCM GI-HS °C	ΔCH_4 D-O ppbv	SDGVM GI-HS ppbv	LPJ-SDGVM GI-HS ppbv
LGM	–	−20	−19.6	–	7.3	–	44	−9, 13
14 kyr	1	−15	−10.7	11	8.8	170	107	−10, −5
38 kyr	8	−18	−16.1	11	8.2	140	94	−18, −1
44 kyr	11	−20	−15.7	15	9.1	112	87	−17, 8
60 kyr	17	−19	−15.2	12	9.4	185	80	−10, 6

ΔT and ΔCH_4 are derived from ice-core reconstructions. The LGM case is included for comparison with the work of Hopcroft et al. (2011). GCM Greenland anomalies are averaged over 60–20° W by 70–80° N. LPJ-SDGVM shows the difference between LPJ-WHyMe and SDGVM over the region ≥45° N. The range encompasses two scenarios of peat area (standard and with extra peat in Europe and North America).

CPD
9, 3519–3561, 2013

Table 2. Principal differences between LPJ-WHyMe and SDGVM relevant to the simulation of CH_4 emissions.

	SDGVM	LPJ-WHyMe
Carbon cycle	Upland 6 PFTs	Wetland 2 PFTs
Carbon substrate	Multi-pool H_r	Multi-pool H_r
Temperature dependence	$Q_{10} = 1.5$	Activation energy
Transport pathways	No	Ebullition, diffusion, plant
Soil thermodynamics	No	Vertically discretised to 10m
Freeze-thaw	No	Yes
Hydrology	Following Cao et al. (1996)	Following Granberg et al. (1999)
Potential wetland	From soil moisture	Prescribed peat area
Nitrogen cycle	CENTURY model	No

H_r denotes soil heterotrophic respiration.

CPD
9, 3519–3561, 2013

Table 3. CH_4 emissions in LPJ-WHyMe and as inferred from observations. *no Sib* indicates that the Siberia peat complex is omitted and *NA + EU* denotes extra peatland areas introduced in North America and Europe as described in the main text. All forcing climates are as simulated directly by FAMOUS, except LPJ-WHyMe (CRU) which is forced with regridded 1961–1990 mean climatological observations (New et al., 1999). ±1.0 Sv denotes the transient LGM simulation with double the magnitude of freshwater forcing.

Time	Model/obs	Expt	$[CO_2]$	Area	CH_4 emissions			
			ppmv	10^6 km^2 Eq	Tg CH_4 yr^{-1} Eq	HS	GI	GI-HS
PI	obs/inversion			2.99–4.0[a]	33 ± 18[b]	–	–	–
	LPJ-WHyMe (CRU)		280	3.2	31.0	–	–	–
	LPJ-WHyMe	PI control	280	3.2	33.6	–	–	–
LGM	LPJ-WHyMe	LGM control	185	2.2	1.9	0.6	3.5	2.8
		LGM+PI CO_2	280	2.2	4.0	2.0	6.2	4.2
		no Sib	185	0.32	0.9	0.1	1.6	1.5
		no Sib+NA+EU		1.1	6.2	3.9	11.9	8.0
		+NA+EU		3.0	7.3	4.4	13.5	9.1
LGM	LPJ-WHyMe	±1.0 Sv	185	2.2	1.9	0.4	4.0	3.6
14 kyr	LPJ-WHyMe	14kyr control	237	2.2	11.1	7.6	15.1	7.5
		no Sib		0.25	4.0	1.8	6.1	4.3
		no Sib+NA+EU		0.42	14.0	12.1	18.4	6.2
		+NA+EU		2.37	21.1	17.9	26.3	8.4
38 kyr	LPJ-WHyMe	38kyr control	211	2.1	4.9	2.2	5.9	3.7
		no Sib		0.15	1.2	0.4	2.1	1.7
		no Sib+NA+EU		0.31	10.8	7.8	14.6	6.8
		+NA+EU		2.26	14.4	9.7	19.1	9.4
44 kyr	LPJ-WHyMe	44 kyr control	213	2.3	4.6	3.0	6.1	3.1
		no Sib		0.3	1.0	0.7	2.0	1.2
		no Sib+NA+EU		1.1	10.1	8.3	15.0	6.7
		NA+EU		3.1	13.6	10.6	18.9	8.2
60 kyr	LPJ-WHyMe	60 kyr control	211	2.3	4.2	2.5	5.8	3.3
		no Sib		0.3	1.2	0.7	2.2	1.5
		no Sib+NA+EU		1.1	10.1	8.1	14.6	6.5
		+NA+EU		3.1	13.1	10.0	17.6	7.7

[a] Spahni et al. (2011); Yu et al. (2010); [b] Chen and Prinn (2006).

CPD
9, 3519–3561, 2013

Table 4. CH_4 emissions in sensitivity simulations with modified model versions and ≥45° N in SDGVM (this study and Hopcroft et al., 2011). *h*, R_h and *T* signify hydrology, soil heterotrophic respiration and soil temperature respectively. These fields are read into the modified versions of SDGVM from LPJ-WHyMe. Wetland area in SDGVM is calculated from the area with the water table depth ≥ 0cm, but in other models is the area of prescribed peatland.

Time	Model	$[CO_2]$	Area	CH_4 emissions			
		ppmv	10^6 km^2	Tg CH_4 yr^{-1}			
			Eq	Eq	HS	GI	GI-HS/EQ
PI	LPJ-WHyMe	280	3.2	33.6	–	–	–
	SDGVM		18.3	32.7	–	–	–
LGM	LPJ-WHyMe	185	2.2	1.9	0.6	3.5	153 %
	SDGVM-LPJ-hR_hT		2.2	2.1	0.1	3.5	158 %
	SDGVM-LPJ-hR_h		2.2	3.6	2.0	4.8	79 %
	SDGVM-LPJ-h		2.2	13.2	9.8	14.5	36 %
	SDGVM		15.0	13.3	10.7	16.1	40 %
LGM±1.0Sv	LPJ-WHyMe	185	2.2	1.9	0.4	4.0	190 %
	SDGVM-LPJ-hR_hT		2.2	2.2	0.03	4.04	186 %
	SDGVM-LPJ-hR_h		2.2	3.5	1.4	5.3	112 %
	SDGVM-LPJ-h		2.2	13.2	8.6	14.9	48 %
	SDGVM		15.0	13.4	10.1	16.9	51 %
14kyr	LPJ-WHyMe	237	2.2	11.1	7.6	15.1	68 %
	SDGVM-LPJ-hR_hT		2.2	9.6	4.9	13.6	90 %
	SDGVM-LPJ-hR_h		2.2	16.7	14.8	19.7	34 %
	SDGVM-LPJ-h		2.2	33.0	28.7	37.1	26 %
	SDGVM		18.3	33.9	27.7	38.2	32 %
38kyr	LPJ-WHyMe	211	2.1	4.9	2.2	5.8	74 %
	SDGVM-LPJ-hR_hT		2.1	3.0	0.7	3.9	111 %
	SDGVM-LPJ-hR_h		2.1	9.1	5.1	8.6	39 %
	SDGVM-LPJ-h		2.1	22.3	17.4	24.4	31 %
	SDGVM		16.6	20.7	16.6	23.9	35 %
44kyr	LPJ-WHyMe	213	2.3	4.6	3.0	6.1	68 %
	SDGVM-LPJ-hR_hT		2.3	2.7	1.5	5.4	95 %
	SDGVM-LPJ-hR_h		2.3	8.4	5.4	9.7	36 %
	SDGVM-LPJ-h		2.3	21.4	17.2	22.3	24 %
	SDGVM		16.0	19.2	15.5	21.7	33 %
60kyr	LPJ-WHyMe	211	2.3	4.2	2.5	5.8	79 %
	SDGVM-LPJ-hR_hT		2.3	2.7	1.5	5.4	149 %
	SDGVM-LPJ-hR_h		2.3	8.4	5.4	9.7	51 %
	SDGVM-LPJ-h		2.3	25.4	20.4	27.2	27 %
	SDGVM		17.5	22.3	18.6	26.0	33 %

CPD
9, 3519–3561, 2013

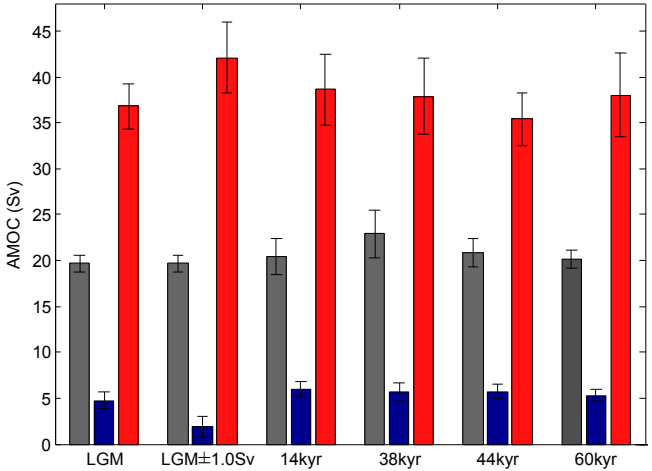

Fig. 1. 30 yr mean ± 1 standard deviation Atlantic meridional overturning circulation (AMOC) values for the 3 phases of each climate simulation: grey EQ (equilibrium), blue HS (Heinrich Stadial-like) and red GI (Greenland interstadial-like).

CPD
9, 3519–3561, 2013

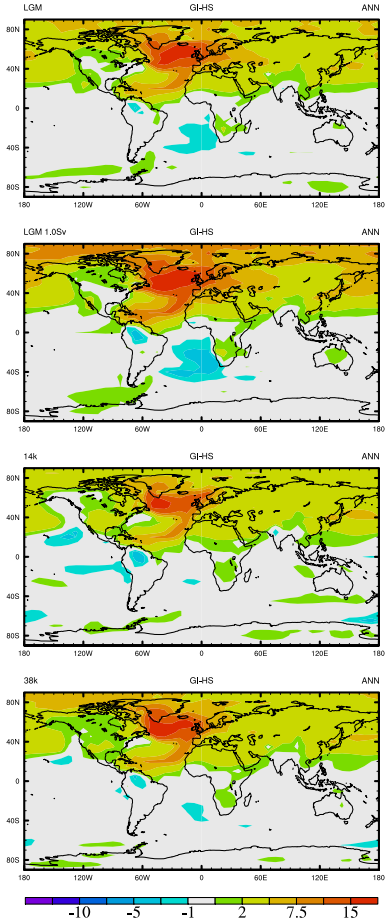

Fig. 2. Annual mean GI-HS surface temperature anomalies (°C) in 4 model runs.

CPD
9, 3519–3561, 2013

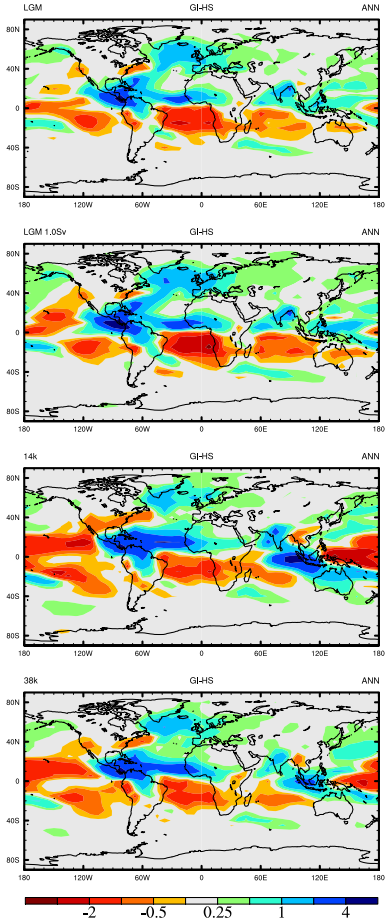

Fig. 3. Annual mean GI-HS precipitation anomalies (mm day^{-1}) in 4 model runs.

CPD
9, 3519–3561, 2013

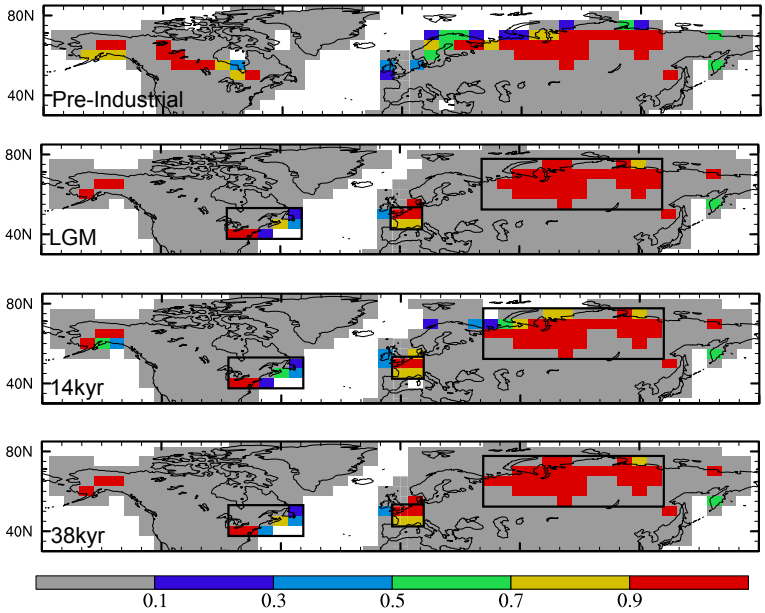

Fig. 4. Prescribed peat grid-cells in the pre-industrial, 21 14 and 38 kyr simulations. Boxes indicate area of peat removed (for Siberia) or additionally prescribed (for North West America and Europe) as summarised in Table 3.

CPD
9, 3519–3561, 2013

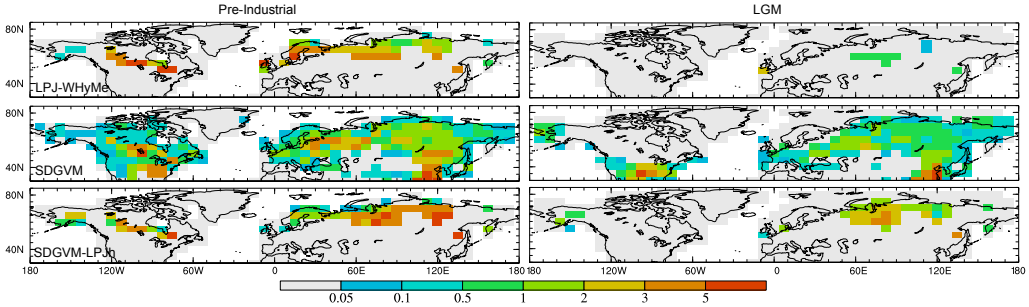

Fig. 5. CH_4 emissions for PI and LGM conditions for LPJ-WHyMe, SDGVM and SDGVM-LPJ-h. Units of $gCH_4\,m^{-2}\,yr^{-1}$, including a correction for the fractional land area in coastal gridcells.

CPD
9, 3519–3561, 2013

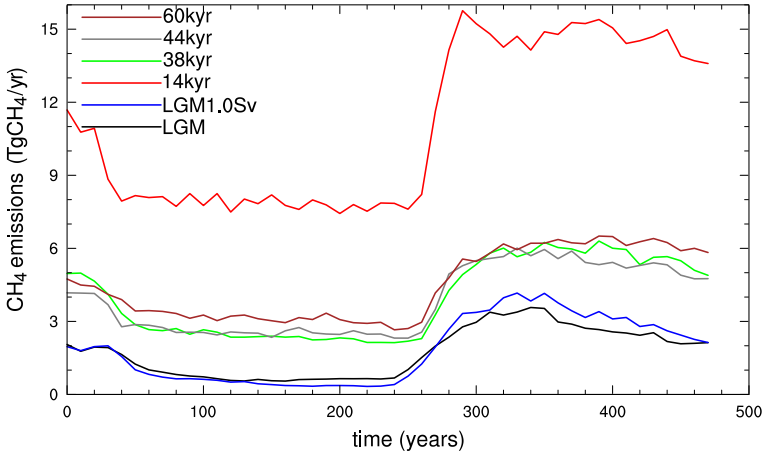

Fig. 6. Decadally averaged mean CH_4 emission timeseries in LPJ-WHyMe for the 5 different palaeoclimate simulations.

CPD
9, 3519–3561, 2013

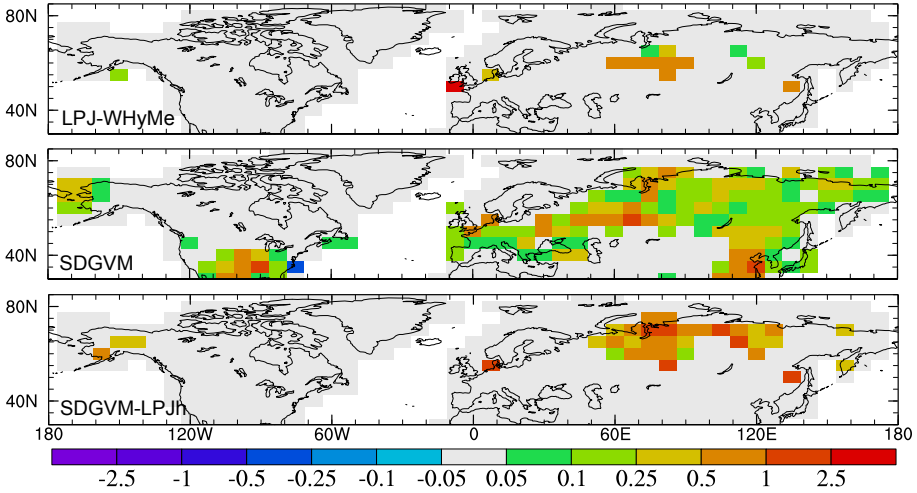

Fig. 7. CH_4 emission anomalies for GI-HS for LGM conditions in LPJ-WHyMe, SDGVM and SDGVM-LPJ-h. Units of $gCH_4\,m^{-2}\,yr^{-1}$, including a correction for the fractional land area in coastal gridcells.

CPD
9, 3519–3561, 2013

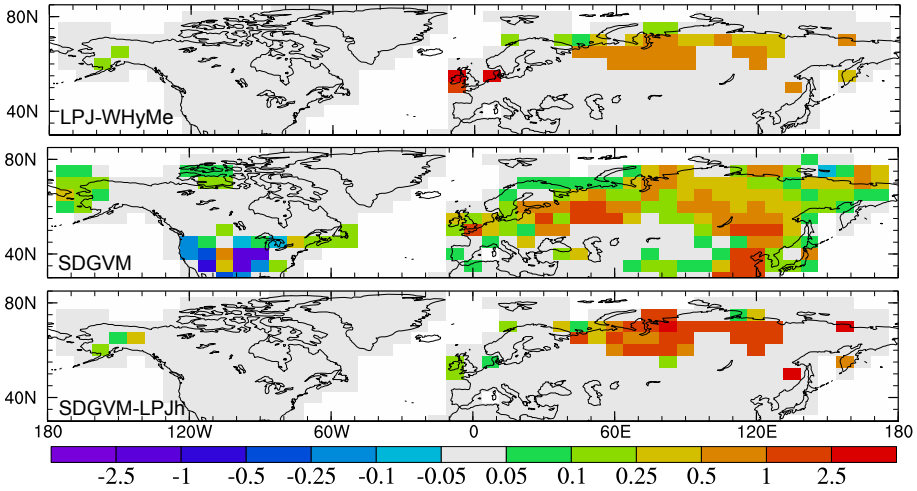

Fig. 8. CH_4 emission anomalies for GI-HS for 14kyr conditions in LPJ-WHyMe, SDGVM and SDGVM-LPJ-h. Units of $gCH_4\,m^{-2}\,yr^{-1}$, including a correction for the fractional land area in coastal gridcells

CPD
9, 3519–3561, 2013